
SSCBench: A Large-Scale 3D Semantic Scene Completion Benchmark for Autonomous Driving

Yiming Li^{1,*} Sihang Li^{1,*} Xinhao Liu^{1,*} Moonjun Gong^{1,*}
Kenan Li¹ Nuo Chen¹ Zijun Wang¹ Zhiheng Li¹ Tao Jiang²
Fisher Yu³ Yue Wang⁴ Hang Zhao² Zhiding Yu⁴ Chen Feng^{1,†}
¹NYU ²Tsinghua University ³ETH Zurich ⁴NVIDIA

Abstract

Semantic scene completion (SSC) is crucial for holistic 3D scene understanding by jointly estimating semantics and geometry from sparse observations. However, progress in SSC, particularly in autonomous driving scenarios, is hindered by the scarcity of high-quality datasets. To overcome this challenge, we introduce SSCBench, a comprehensive benchmark that integrates scenes from widely-used automotive datasets (e.g., KITTI-360, nuScenes, and Waymo). SSCBench follows an established setup and format in the community, facilitating the easy exploration of the camera- and LiDAR-based SSC across various real-world scenarios. We present quantitative and qualitative evaluations of state-of-the-art algorithms on SSCBench and commit to continuously incorporating novel automotive datasets and SSC algorithms to drive further advancements in this field. Our resources are released on <https://github.com/ai4ce/SSCBench>.

1 Introduction

Holistic 3D scene understanding is crucial for autonomous vehicles to navigate complex environments. However, creating a comprehensive representation of a 3D scene poses significant challenges due to occlusions and sparse measurements caused by limited sensing capabilities [4, 5]. One effective solution termed 3D semantic scene completion (SSC) [6] aims to learn the mapping from a sparse and partial observation to a complete 3D representation. The output volume combines occupancy and semantic information for improved autonomous vehicle planning in complex real-world situations.

One critical hurdle in 3D semantic scene completion is the generation of accurate ground truth labels, particularly in the context of large-scale driving scenes. In literature, this challenge has been partially addressed by the pioneer SemanticKITTI [7]. By aggregating future LiDAR sweeps, SemanticKITTI successfully unveils 3D surfaces that were previously concealed due to self-occlusion. As a result, a relatively comprehensive 3D scene representation can be captured as the ground truth label for SSC.

Although SemanticKITTI provides a valuable resource to learn sparse-to-dense mapping, its limited scale and diversity hamper the development of more powerful and generalizable SSC models. Furthermore, a notable limitation of SemanticKITTI is its omission of dynamic objects during ground truth generation, leading to inaccurate labels. Hence, there is an urgent need for diverse SSC datasets with accurate ground truth to drive advancements in autonomous vehicle perception.

To this end, we propose SSCBench, a large-scale benchmark composed of diverse driving scenes sourced from well-established automotive datasets, including KITTI-360 [1], nuScenes [2], and Waymo [3], as shown in Fig. 1. SSCBench offers datasets in a format compatible with SemanticKITTI, facilitating their effortless adoption by the community to explore camera- and LiDAR-based SSC in various real-world scenarios. Furthermore, to improve label accuracy, we leverage the 3D bounding

*Equal contribution

†The corresponding author is Chen Feng cfeng@nyu.edu

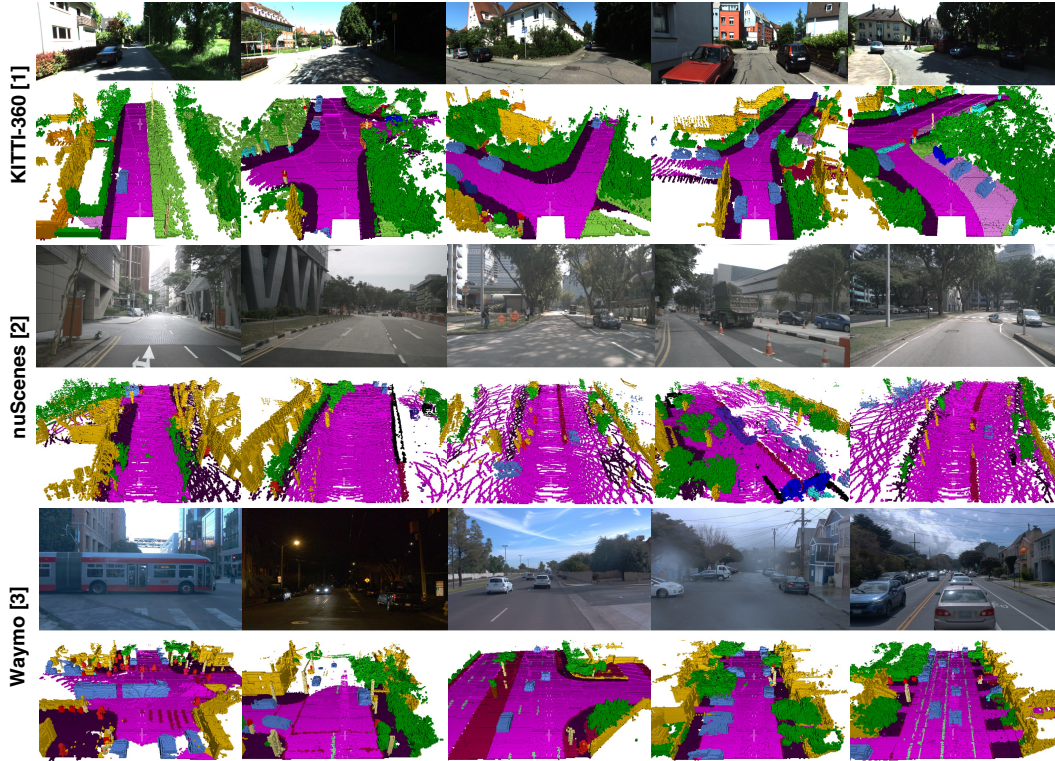


Figure 1: **Visualizations of SSCBench** derived from KITTI-360 [1], nuScenes [2], and Waymo [3]. We showcase accurate 3D semantic scene completion ground truth for rich driving scenarios. We commit to incorporating novel datasets for further development.

box labels provided in these datasets to synchronize measurements of dynamic objects. We report quantitative and qualitative performances of state-of-the-art algorithms on SSCBench. We make our code and datasets publicly available and will continue incorporating novel automotive datasets and SSC algorithms to promote further development in SSC and autonomous vehicle perception.

2 Related Works

Dataset and Benchmark for Autonomous Driving. Autonomous driving research thrives on high-quality datasets, which serve as the lifeblood for training and evaluating perception [2], prediction [8], and planning algorithms [9]. In 2012, the pioneering KITTI dataset sparked a revolution in autonomous driving research, unlocking a multitude of tasks including object detection, tracking, mapping, and optical/depth estimation [10–14]. Since then, the research community has embraced the challenge, giving rise to a wealth of datasets. These datasets push the boundaries of autonomous driving research by addressing challenges posed by multimodal fusion [2], multi-tasking learning [15, 1], adverse weather [16], collaborative driving [17–20], repeated driving [21], and dense traffic scenarios [22, 23], *etc.* There are several impactful and widely-used driving datasets such as KITTI-360 [1], nuScenes [2], and Waymo [3]. They provide LiDAR and camera recordings as well as point cloud semantics and bounding box annotations, as summarized in Table 1. Therefore, we can create accurate ground truth labels for 3D semantic scene completion by superimposing multiple semantic point clouds and leveraging the 3D boxes to handle dynamic objects.

BEV Perception in Autonomous Driving. Bird’s-eye-view (BEV) perception in autonomous driving has garnered significant attention [30, 31]. While traditional methods mainly operate within a perspective view, the increasing complexity of sensor configurations has necessitated the integration of multimodal features in a unified BEV view. DETR3D [32] is proposed as a pioneering vision-based 3D detector, leveraging camera projection matrices to establish connections between learnable 3D object queries and 2D images, enabling end-to-end 3D bounding box prediction without non-maximum suppression. Subsequently, extensive research efforts have been dedicated to the exploration of

Table 1: **Overview of widely-used autonomous driving datasets with multimodal sensors.** C denotes camera and L denotes LiDAR. Most datasets provide 3D bounding box annotations for 3D object detection, yet only a few of them provide semantic labels for the LiDAR point cloud due to the high cost. Note that ApolloScape [24] only provides 3D semantic labels for the static environment.

Datasets	Year	Sensors	Annotations	# Fr. with Pts Ann.	Sequential
KITTI [10]	CVPR 2012	C&L	3D Bbox	N.A.	✗
SemanticKITTI [7]	ICCV 2019	C&L	3D Pts.	20K	✓
nuScenes [2]	CVPR 2019	C&L	3D Bbox	N.A.	✓
Panoptic nuScenes [25]	RA-L 2022	C&L	3D Pts.	40K	✓
Waymo [3]	CVPR 2020	C&L	3D Bbox&Pts.	230K	✓
KITTI-360 [1]	T-PAMI 2022	C&L	3D Bbox&Pts.	100K	✓
ApolloScape [24]	T-PAMI 2019	C&L	3D Bbox&Pts.	N.A.	✓
Argoverse [26]	CVPR 2019	C&L	3D Bbox	N.A.	✓
ONCE [27]	NeurIPS 2021	C&L	3D Bbox	N.A.	✓
Lyft Level 5 [28]	2019	C&L	3D Bbox	N.A.	✓
A*3D [22]	ICRA 2020	C&L	3D Bbox	N.A.	✓
A2D2 [29]	2020	C&L	3D Bbox	N.A.	✗

BEV perception such as multi-task BEV perception [33], multimodal BEV detection [34, 35], BEV tracking [36, 37], collaborative BEV segmentation [38], and scene generation [39]. BEV perception offers unique advantages such as fusion-friendly representation and compatibility with planning. However, it faces limitations in handling overhangs and vertical structures, as well as the lack of fine-grained information due to projecting 3D information onto a 2D grid.

3D Semantic Scene Completion for Autonomous Driving. Limited sensing range poses a challenge to holistic 3D scene understanding. Researchers propose multi-agent perception to enrich observations of the scene [40–48]. 3D semantic scene completion (SSC) [6] offers an alternative solution. It completes 3D scene structures within a voxelized 3D volume based on sparse observations, providing a comprehensive scene understanding. Unlike BEV perception, SSC captures volumetric information, accurately representing complex scenes with overhangs and vertical structures. Additionally, it enables detailed analysis, supporting state estimation and safe planning [49–52, 9]. However, existing approaches typically depend on 3D inputs, such as LiDAR point clouds [53–57], while recent vision-centric solutions [58–60] also emerges. However, the development of outdoor SSC is hindered by the lack of datasets, with SemanticKITTI [7] being the only dataset supporting outdoor SSC. Building diverse datasets is imperative to unlock the full potential of SSC for autonomous perception.

3 Dataset Curation

3.1 Revisit of SemanticKITTI

SemanticKITTI [7] extends the odometry dataset of the KITTI vision benchmark [10] by providing point-wise semantic annotations for 22 driving sequences in Karlsruhe, Germany. SemanticKITTI not only supports 3D semantic segmentation but also serves as the first outdoor SSC benchmark. Similar to indoor SSC [61], SemanticKITTI uses voxelized 3D representation widely employed in robotics such as occupancy grid mapping [62]. SemanticKITTI generates ground truth labels through voxelization of a dense semantic point cloud given by rigid registration of multiple LiDAR scans.

SemanticKITTI has two limitations. First, rigid registration with sensor poses can only handle measurements for static environments, resulting in traces produced by dynamic objects such as moving cars as shown in Fig. 2, which can confuse the 3D representation learning [55]. Secondly, it is constrained by the limited scale and lack of diverse geographical coverage. The data collection is confined to a single city, resulting in training, validation, and test sets composed of 3,834, 815, and 3,992 frames, respectively, amounting to a total of 8,641 frames. However, this falls short of the large-scale benchmark necessary for comprehensive evaluation and generalization in the field.

3.2 SSCBench

We aim to establish a large-scale driving benchmark that facilitates the training of robust and generalizable SSC models. To achieve this, we harness well-established and widely-used datasets

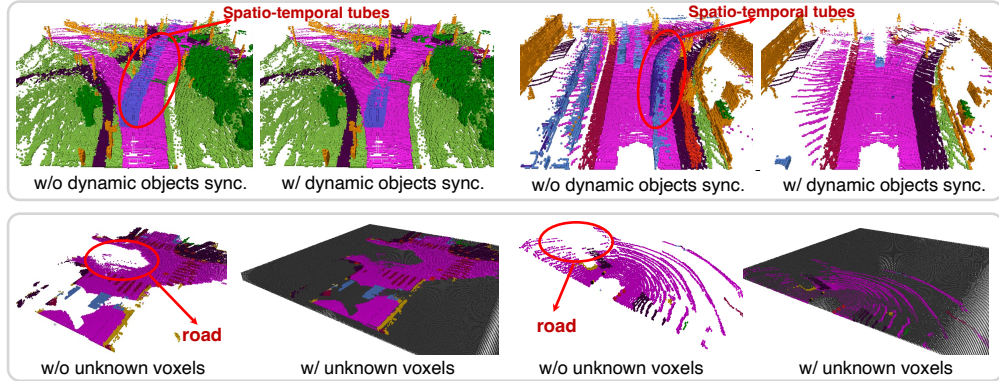


Figure 2: **Top row: dynamic objects synchronization.** Two examples on nuScenes [2] dataset are shown. Spatio-temporal tubes are introduced without handling dynamic objects, leading to inaccurate ground truth labels. **Bottom row: unknown voxels exclusion.** Voxels are marked as unknown (denoted by grey color) when they are occluded by other objects or remain unprobed by the LiDAR.

and integrate them into a unified setup and format. In the following, we introduce three carefully designed datasets, all based on existing data sources, that collectively contribute to our SSCBench.

3.2.1 SSCBench-KITTI-360

KITTI-360 [1] represents a significant advancement in autonomous driving research, building upon the renowned KITTI dataset [10]. It introduces an enriched data collection framework with diverse sensor modalities as well as panoramic viewpoints (a perspective stereo camera plus a pair of fish-eye cameras), and provides comprehensive annotations including consistent 2D and 3D semantic instance labels as well as 3D bounding primitives. The dense and coherent labels not only support established tasks such as segmentation and detection but also enable novel applications like semantic SLAM [63] and novel view synthesis [64]. While KITTI-360 includes point cloud-based semantic scene completion, the prevalent methodology for SSC remains centered around voxelized representations [54, 53, 58, 59, 6, 55], which exhibit broader applicability in robotics.

KITTI-360 covers a driving distance of 73.7km, comprising 300K images and 80K laser scans. While adhering to KITTI’s forward-facing camera setup, it offers greater geographical diversity and demonstrates minimal trajectory overlap with the original KITTI dataset. Leveraging the open-source training and validation set, we build SSCBench-KITTI-360 consisting of 9 long sequences. To reduce redundancy, we sample every 5 frames following the SemanticKITTI SSC benchmark. The training set includes 8,487 frames from scenes 00, 02-05, 07, and 10, while the validation set comprises 1,812 frames from scene 06. The testing set comprises 2,566 frames from scene 09. In total, the dataset contains 12,865 (~ 13 K) frames, surpassing the scale of SemanticKITTI by ~ 1.5 times.

3.2.2 SSCBench-nuScenes

Unlike KITTI’s forward-facing camera setup, nuScenes [2] captures a complete 360-degree view around the ego vehicle. It provides a diverse range of multimodal sensory data, including camera images, LiDAR point clouds, and radar data, gathered in Boston and Singapore. nuScenes offers meticulous annotations for complex urban driving scenarios, including diverse weather conditions, construction zones, and varying illumination. Later on, panoptic nuScenes [25] extends the original nuScenes dataset with semantic and instance labels. With comprehensive metrics and evaluation protocols, nuScenes is widely employed in the autonomous driving research [65, 9, 66, 60]

The nuScenes dataset consists of 1K 20-second scenes with labels provided only for the training and validation set, totaling 850 scenes. From the publicly available 850 scenes, we allocate 500 scenes for training, 200 scenes for validation, and 150 scenes for testing. This distribution results in 20,064 frames for training, 8,050 frames for validation, and 5,949 frames for testing, totaling 34,078 frames (~ 34 K). This scale is approximately four times that of SemanticKITTI. As nuScenes only provides annotations for keyframes at a frequency of 2Hz, there is no downsampling in SSCBench-nuScenes.

3.2.3 SSCBench-Waymo

The Waymo dataset [3], collected from various locations in the United States, offers a large-scale collection of multimodal sensor recordings. Waymo provides 5 cameras with a combined horizontal

field of view of ~ 230 degrees, slightly smaller than nuScenes. The data is captured in diverse conditions across multiple cities, including San Francisco, Phoenix, and Mountain View, ensuring broad geographical coverage within each city. It consists of 1000 scenes for training and validation, as well as 150 scenes for testing, with each scene spanning 20 seconds.

To construct SSCBench-Waymo, we utilize the open-source training and validation scenes and redistribute them into sets of 500, 298, and 202 scenes for training, validation, and testing, respectively. In order to reduce redundancy and training time for our benchmark, we downsample the original data by a factor of 10. This downsampling results in a training set of 10,011 frames, a validation set of 5,936 frames, and a test set of 4,038 frames, totaling 19,985 frames ($\sim 20K$).

3.3 Construction Pipeline

Prerequisites. To establish SSCBench, a driving dataset with multimodal recordings is required for LiDAR-based or camera-based SSC. The dataset should include sequentially-collected 3D LiDAR point clouds with accurate sensor poses for geometry completion, per-point semantic annotations for semantic scene understanding, and 3D bounding annotations to handle dynamic instances.

Aggregation of point clouds. To generate a complete representation, our approach involves superimposing an extensive set of laser scans within a defined region in front of the vehicle. In short sequences like nuScenes and Waymo, we utilize future scans with measurements from the corresponding region to create a dense semantic point cloud. However, in long sequences like KITTI-360, which feature multiple loop closures, we incorporate all spatial neighboring point clouds in addition to the temporal neighborhood. Accurate sensor poses, provided by advanced SLAM systems [67], greatly facilitate the aggregation of point clouds for the static environment. As for dynamic objects, we handle them separately by transforming and aggregating points based on bounding box annotations.

Voxelization of aggregated point clouds. Voxelization is to discretize a continuous 3D space into a regular grid structure composed of volumetric elements called voxels, enabling the conversion of unstructured data into a structured format that can be efficiently processed by convolutional neural networks (CNNs) or vision transformers (ViTs). Voxelization introduces a trade-off between spatial resolution and memory consumption and offers a flexible and scalable representation for 3D perception [68, 69, 59]. For easy integration, SSCBench adheres to SemanticKITTI’s setup, with a volume extending 51.2m ahead, 25.6m on each side, and 6.4m in height. Voxel resolution is 0.2m, resulting in a $256 \times 256 \times 32$ voxel volume. Labels for each voxel are determined by majority voting among labeled points within it, while empty voxels are marked accordingly if no points are present.

Exclusion of unknown voxels. Capturing complete 3D outdoor dynamic scenes is nearly impossible without ubiquitous scene sensing, so we only consider *visible and probed* voxels from all viewpoints during training and evaluation. Specifically, we first employ ray tracing from different perspectives to identify and remove occluded voxels within objects or behind walls. Furthermore, in datasets with sparse sensing, where numerous voxels remain unprobed, we remove these unknown voxels during training and evaluation to enhance the reliability of the ground truth labels as shown in Fig. 2.

3.4 Dataset Statistics

We show dataset statistics in Fig. 3. The dataset label distribution reveals noticeable domain gaps among various cities. Specifically, KITTI-360 and SemanticKITTI exhibit similar label distributions due to being captured within the same city in German. However, nuScenes and Waymo collected in the US and Singapore demonstrate distinct label distributions. Furthermore, SSCBench stands out for its larger scale in comparison to SemanticKITTI. For instance, SSCBench comprises 7.7 times more frames than SemanticKITTI, and its collection of driving sequences is also more diverse.

4 Benchmark Results

4.1 Experimental Setup

Methods and implementation. We carefully select two LiDAR-based methods [61, 53] and two camera-based methods [58, 59] for our comparative analysis. These methods are chosen based on their widespread adoption, and cutting-edge performance in the field. We utilize the public codebase of these methods, running them with their default setups to ensure consistency. However, we make necessary adjustments to data loaders and batch sizes during the benchmarking process, aiming

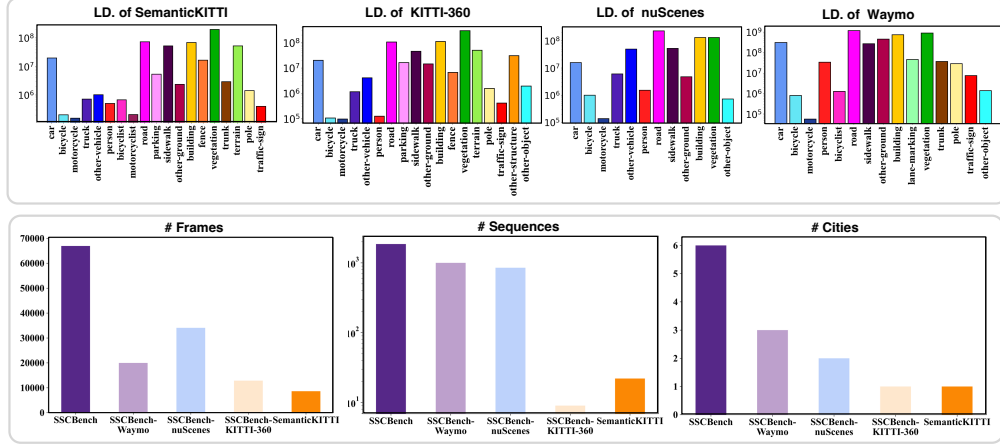


Figure 3: **Statistical Analysis.** Top row: Label Distribution (LD.) of different datasets. Bottom row: scale comparisons between SSCBench and SemanticKITTI.

Methods	VoxFormer-S [59]			MonoScene [58]			LMSCNet [53]			SSCNet [61]		
	12.8m	25.6m	51.2m	12.8m	25.6m	51.2m	12.8m	25.6m	51.2m	12.8m	25.6m	51.2m
Range	12.8m	25.6m	51.2m	12.8m	25.6m	51.2m	12.8m	25.6m	51.2m	12.8m	25.6m	51.2m
IoU (%)	55.45	46.36	38.76	54.65	44.70	37.87	65.34	57.43	47.35	70.97	62.96	53.58
Precision (%)	66.10	61.34	58.52	65.88	59.96	56.73	77.14	73.07	72.77	78.17	72.25	69.63
Recall (%)	77.48	65.48	53.44	76.24	63.72	53.26	81.03	72.85	57.55	88.52	83.05	69.92
mIoU	18.17	15.4	11.91	20.29	16.18	12.31	20.04	17.57	13.65	24.01	21.40	16.95
■ car (2.85%)	29.41	25.08	17.84	30.83	26.35	19.34	37.49	31.71	20.91	50.02	44.47	31.95
■ bicycle (0.01%)	2.73	1.73	1.16	1.94	0.83	0.43	0.00	0.00	0.00	0.00	0.00	0.00
■ motorcycle (0.01%)	1.97	1.47	0.89	3.25	1.30	0.58	0.00	0.00	0.00	1.02	0.36	0.17
■ truck (0.16%)	6.08	6.63	4.56	14.83	12.18	8.02	0.65	0.46	0.26	14.67	13.69	10.29
■ other-veh. (5.75%)	3.71	3.56	2.06	6.08	4.30	2.03	1.49	1.01	0.58	0.00	0.00	0.00
■ person (0.02%)	2.86	2.20	1.63	2.06	1.26	0.86	0.00	0.00	0.00	0.26	0.13	0.07
■ road (14.98%)	66.10	58.58	47.01	68.60	59.93	48.35	77.35	74.32	62.95	78.03	75.96	65.70
■ parking (2.31%)	18.44	13.52	9.67	24.32	16.4	11.38	25.56	20.43	13.51	29.60	24.51	17.33
■ sidewalk (6.43%)	38.00	33.63	27.21	44.43	36.05	28.13	51.20	44.42	33.51	56.60	51.40	41.24
■ other-grnd (2.05%)	4.49	4.04	2.89	5.76	4.82	3.32	0.41	0.32	0.20	6.88	5.36	3.22
■ building (15.67%)	41.12	38.24	31.18	45.40	40.60	32.89	58.66	54.08	43.67	62.14	54.04	44.41
■ fence (0.96%)	8.99	7.43	4.97	9.79	5.91	3.53	1.66	0.71	0.33	13.53	11.06	6.77
■ vegetation (41.99%)	45.68	35.16	28.99	42.98	32.75	26.15	55.87	48.52	40.01	59.28	51.96	43.72
■ terrain (7.10%)	24.70	18.53	14.69	31.96	21.63	16.75	41.96	34.15	26.80	40.80	34.84	28.87
■ pole (0.22%)	8.84	8.16	6.51	9.28	8.45	6.92	0.00	0.00	0.00	1.09	1.19	0.78
■ traf.-sign (0.06%)	9.15	9.02	6.92	8.58	7.67	5.67	0.00	0.00	0.00	0.90	1.16	0.75
■ other-struct. (4.33%)	10.31	7.02	3.79	9.18	6.76	4.20	9.87	7.09	3.63	14.80	12.98	8.60
■ other-obeject (0.28%)	4.40	3.27	2.43	5.86	4.49	3.09	0.0028	0.0007	0.0003	1.13	1.07	0.67

Table 2: **Quantitative comparison on SSCBench-KITTI-360.** We report the performances with respect to different ranges (12.8m, 25.6m, and 51.2m). We provide both geometric (IoU) and semantic (mIoU) metrics. The top three performances are marked by **red**, **green**, and **blue** respectively.

to integrate seamlessly with SSCBench and optimize computational resources. In this section, we train, validate, and test these methods individually on each subset of SSCBench. Furthermore, we provide a unified benchmark in the supplementary materials where models are trained on one subset and tested on others, *e.g.*, train on SSCBench-KITTI-360 and test on SSCBench-nuScenes and SSCBench-Waymo. This additional benchmark serves to highlight and compare the cross-domain generalizability of these methods.

Evaluation metrics. We adopt the intersection over union (IoU) for evaluating geometry completion and the mean IoU (mIoU) of each class for evaluating semantic segmentation, following the existing SSC methods. We also report the ratio of different classes in the dataset to better understand the relationship between IoU and mIoU. We report the performances across three distinct scales of volume: $12.8 \times 12.8 \times 6.4 \text{m}^3$, $25.6 \times 25.6 \times 6.4 \text{m}^3$, and $51.2 \times 51.2 \times 6.4 \text{m}^3$. The design of this multi-scale evaluation emphasizes the area directly in the vehicle’s anticipated forward trajectory. This approach provides insightful data on performance relative to the perception range, which is crucial for many downstream tasks including planning and navigation [9].

Methods	VoxFormer-S [59]			MonoScene [58]			LMSCNet [53]			SSCNet [61]		
Range	12.8m	25.6m	51.2m	12.8m	25.6m	51.2m	12.8m	25.6m	51.2m	12.8m	25.6m	51.2m
IoU (%)	59.75	39.25	25.16	65.06	44.79	29.63	61.40	36.98	21.09	63.44	43.06	27.64
Precision (%)	85.48	72.33	53.11	88.83	75.95	60.64	92.89	86.48	83.12	84.22	68.89	59.21
Recall (%)	66.5	46.18	32.34	70.84	52.09	36.69	64.03	39.25	22.03	72.00	53.45	34.14
mIoU	8.89	7.05	4.96	18.89	13.59	9.60	22.4	14.19	8.36	25.7	18.24	11.84
■ car (2.47%)	8.23	7.65	4.95	21.95	14.86	10.17	38.62	24.29	14.74	38.36	27.04	18.06
■ bicycle (0.16%)	0.26	0.38	0.29	4.13	2.39	1.70	0.00	0.00	0.00	0.00	0.00	0.00
■ motorcycle (0.02%)	1.56	1.99	1.21	5.86	5.72	3.80	0.00	0.00	0.00	2.24	0.77	0.36
■ truck (0.96%)	4.06	4.05	2.73	17.18	11.55	8.35	18.40	10.32	5.93	26.67	18.89	13.42
■ other-veh. (7.87%)	5.17	4.13	2.45	18.51	11.87	8.74	17.58	13.28	8.52	20.01	14.85	10.35
■ person (0.24%)	2.53	1.71	1.12	10.65	5.66	3.72	13.22	6.37	3.41	18.15	12.25	7.59
■ road (36.97%)	48.79	36.19	23.94	70.6	54.59	38.77	63.39	40.82	24.14	65.28	45.49	28.74
■ sidewalk (8.30%)	17.22	14.45	10.14	32.75	23.03	14.74	26.10	14.29	7.55	35.46	23.23	12.65
■ other-grnd (0.75%)	8.56	6.52	4.06	28.86	19.94	12.58	26.90	15.29	8.40	34.63	22.00	12.65
■ building (21.17%)	2.62	2.30	3.97	5.28	6.51	7.23	36.77	28.94	18.56	35.83	30.44	21.05
■ vegetation (20.97%)	7.62	5.18	4.58	10.79	6.90	5.50	27.87	16.74	9.02	31.81	23.91	16.33
■ other-object (0.11%)	0.02	0.05	0.06	0.29	0.06	0.03	0.00	0.00	0.00	0.00	0.02	0.01

Table 3: **Quantitative comparison on nuScenes.** All metrics and legends follow those in Tab. 2

4.2 Results on SSCBench-KITTI-360

Camera vs. LiDAR. As demonstrated in Table 2, LiDAR-based methods surpass camera-based approaches in all geometric metrics (IoU, precision, and recall) and most of the semantic metrics. This is an expected result, given that camera-based methods must infer 3D scene geometry from 2D images, while LiDAR-based methods directly extract scene geometry from LiDAR input. However, camera-based methods outperform LiDAR-based techniques when dealing with smaller objects that comprise a minuscule fraction of samples ($< 0.5\%$). For classes such as bicycle (■, $0.00 \rightarrow 1.16$), person (■, $0.26 \rightarrow 2.86$), pole (■, $1.09 \rightarrow 9.28$), and traffic sign (■, $0.90 \rightarrow 9.15$), camera-based methods significantly outperform LiDAR-based methods. Despite the low sample frequency of these classes, their identification is vitally important for collision avoidance and traffic understanding.

Same modality. Generally, we notice similar results for methods using the same input modality. SSCNet slightly outperforms LMSCNet, while VoxFormer’s performance is roughly equivalent to that of MonoScene. SSCNet’s marginally superior performance over LMSCNet can be attributed to its larger parameter count (1.03M compared to 0.35M). Moreover, VoxFormer-s’s failure to surpass MonoScene’s performance can be attributed to the subpar performance of the depth estimation model employed in VoxFormer. These off-the-shelf modules [70, 71], primarily trained on KITTI [10], which provide suboptimal depth knowledge leading to uncompetitive SSC performance.

4.3 Results on SSCBench-nuScenes

Camera vs. LiDAR. In SSCBench-nuScenes, we have a relatively sparse LiDAR input. This is due to the sparse LiDAR sensor used in the nuScenes dataset (Velodyne HDL32E) [2]. As a result, we observe from Tab. 3 that image-based methods generally outperform LiDAR-based methods on geometric metrics such as IoU and precision. However, mirroring the result on SSCBench-KITTI-360, image-based methods only have a superior performance on small objects and are suboptimal for the rest. We can conclude from the result that LiDAR-based methods are sensitive to the sparsity of their inputs. Their performance degenerates significantly when the sparse-to-dense task becomes too challenging.

Same modality. Compared with SSCBench-Waymo, MonoScene has a similar superior performance of almost all metrics over VoxFormer on SSCBench-nuScenes. This is because SSCBench-nuScenes has no stereo image data like SSCBench-KITTI-360 and no depth groundtruth. Thus, the depth estimation model (Lite-Mono) [72] utilized in VoxFormer is self-supervised and isn’t fine-tuned on SSCBench-nuScenes, which can not provide satisfactory depth estimations in the context, leading to a decline in VoxFormer’s performance. As for LiDAR-based methods, SSCNet achieves better performance than LMSCNet just like that on SSCBench-KITTI-360. Additionally, we note that SSCNet has better recognition ability for the small object (■ motorcycle, $2.24 \rightarrow 0.00$), which denotes SSCNet’s preferable adaptation for the sparse LiDAR data than LMSCNet.

4.4 Results on SSCBench-Waymo

Camera vs. LiDAR. Unlike SSCBench-nuScenes, SSCBench-Waymo has a very dense LiDAR input because the Waymo dataset contains point cloud data collected from one mid-range and four short-range lidars [3]. Meanwhile, due to memory constraints, we downsample the image input from 1920×1280 to 960×640 . As a result, we can observe from Tab. 4 that the two LiDAR-based methods outperform camera-based methods by a significant margin. The comparison between experiments on SSCBench-Waymo and SSCBench-nuScenes reveals the sensitivity of LiDAR-based methods to the input. Sparse input can lead to performance degradation, while dense input holds the potential for significant improvement.

LiDAR-based methods. Mirroring the results from SSCBench-KITTI-360 and SSCBench-nuScenes, SSCNet generally delivers superior performance compared to LMSCNet on the SSCBench-Waymo dataset, owing to reasons previously discussed. An intriguing trend observed was the negligible performance degradation of both LiDAR-based methods, even as the perception range expanded from 12.8m to 51.2m. This trend can also be attributed to the dense LiDAR input. However, it’s essential to underscore that although a dense LiDAR input leads to satisfactory performance, this 5-LiDAR setting is still costly to common autonomous driving solutions.

Camera-based methods. In line with prior experiments, MonoScene marginally outperforms VoxFormer-S on the majority of evaluation metrics. Duo to the lack of stereo data on the SSCBench-Waymo dataset, the suboptimal depth prior introduced by the self-supervised model [72] is responsible for the deficient performance of VoxFormer as mentioned above. However, the decrease in mIoU is significantly less pronounced than that in IoU as the range increases. Observing class-wise IoU, we note that it can either increase (■ building, 1.71 \rightarrow 10.33), decrease (■ road, 63.07 \rightarrow 40.79), and barely change (■ sidewalk, 18.77 \rightarrow 17.26) as the perception range increases. This pattern explains the divergence between IoU and mIoU, thereby underscoring the importance of both metrics in our evaluation.

4.5 Discussions and Analyses

Impact of LiDAR input density. Our experiments illuminate the impact of LiDAR input density on model performance. In the SSCBench-nuScenes dataset, which features relatively sparse LiDAR input (32 channels), camera-based methods outperform LiDAR-based methods on geometric metrics. However, in the SSCBench-Waymo dataset, which benefits from dense LiDAR input (64 channels, 5 LiDARs), LiDAR-based methods vastly outperform camera-based methods. The sensitivity of LiDAR-based methods to input becomes evident, with advantages seen in dense input and notable performance degradation in sparse input. This highlights the need for future research in developing robust LiDAR-based methods that can mitigate degradation while capitalizing on the benefits.

Performance across perception ranges. As the perception range expands, all methods generally experience a decrease in performance due to increased complexity and uncertainty in larger volumes. However, LiDAR-based methods, specifically in SSCBench-Waymo, demonstrate minimal performance degradation. This trend, likely attributed to the dense LiDAR input, highlights their ability to maintain stable performance across varying perception ranges. It underscores the potential benefits of dense LiDAR data collection, albeit with increased cost and computational demand. Additionally, this trend emphasizes the need for further research to enhance LiDAR data density and advance depth estimation for camera-based methods, improving their scalability to larger perception ranges.

Comparison with SemanticKITTI. We notice significant divergence when we compare our experiment result on SSCBench to those reported on SemanticKITTI [7] (we refer readers to the VoxFormer [59] for more details). While VoxFormer performs very well in terms of IoU, mIoU, and many class IoUs on SemanticKITTI, it does not adapt very well to the diverse datasets in our SSCBench. This divergence can largely be attributed to the fact that the depth estimation module in VoxFormer, which is highly effective on SemanticKITTI, falls short on SSCBench. Furthermore, LMSCNet, which tends to have better geometric performance than SSCNet on SemanticKITTI, shows the opposite trend on SSCBench. These discrepancies underscore two essential points. First, they highlight the importance of SSCBench, which provides diverse and challenging real-world scenarios, enabling comprehensive evaluations. Second, they emphasize the need for generalizable methods that can maintain high performance across varied environments, not just on a single dataset.

Methods	VoxFormer-S [59]			MonoScene [58]			LMSCNet [53]			SSCNet [61]		
Range	12.8m	25.6m	51.2m	12.8m	25.6m	51.2m	12.8m	25.6m	51.2m	12.8m	25.6m	51.2m
IoU (%)	60.36	44.09	36.36	62.44	45.36	36.81	89.19	89.19	89.04	85.26	85.34	85.43
Precision (%)	75.95	62.90	52.00	79.03	63.16	52.11	94.83	94.84	94.74	88.62	88.71	88.83
Recall (%)	75.03	59.58	54.72	74.84	61.67	55.62	93.75	93.73	93.67	95.74	95.74	95.7
mIoU	9.65	10.11	9.46	12.39	12.26	10.54	39.10	39.05	38.58	42.37	42.17	41.63
■ car (7.65%)	14.60	17.13	14.58	18.18	17.82	14.54	74.13	74.99	75.21	68.05	69.36	69.97
■ bicycle (0.02%)	0.13	0.38	0.36	0.91	0.72	1.36	0.00	0.00	0.00	17.04	14.70	13.23
■ motorcycle (0.001%)	0.00	0.05	0.02	0.04	0.14	0.03	0.00	0.00	0.00	0.00	0.00	0.00
■ person (0.84%)	8.59	6.61	5.20	12.76	9.23	6.59	61.47	59.75	58.22	61.13	60.00	58.32
■ bicyclist (0.03%)	0.95	2.73	1.83	0.61	3.23	3.01	0.16	0.26	0.19	15.13	15.81	15.37
■ road (29.62%)	63.07	49.46	40.79	66.34	53.71	42.51	76.19	76.77	76.29	75.07	75.65	75.40
■ sidewalk (6.65%)	18.77	18.01	17.26	26.57	24.14	19.82	51.53	50.96	51.07	52.07	51.75	51.63
■ other-grnd (11.40%)	8.05	13.17	15.68	17.45	20.42	18.96	51.29	51.49	51.30	51.90	52.15	52.12
■ building (18.38%)	1.71	5.59	10.33	7.78	13.48	12.55	72.08	72.01	71.63	70.61	70.51	70.15
■ lane-marking (1.15%)	11.93	15.42	13.86	12.19	15.51	14.43	10.63	10.19	9.12	14.67	14.33	13.15
■ vegetation (22.41%)	9.72	9.72	11.34	10.03	10.18	11.48	73.67	73.55	73.30	71.06	71.03	70.93
■ trunk (0.90%)	2.14	2.95	2.49	3.35	3.52	2.88	35.01	35.06	34.69	35.80	35.83	35.89
■ pole (0.72%)	1.52	3.19	3.10	2.88	3.79	3.48	42.23	42.47	41.58	42.34	42.21	41.88
■ traf.-sign (0.19%)	2.06	3.08	2.71	4.13	3.74	3.59	28.63	28.78	27.24	35.21	34.51	33.07
■ other-objekt (0.03%)	1.50	4.18	2.38	2.7	4.21	2.94	9.54	9.46	8.83	25.46	24.65	23.28

Table 4: Quantitative comparison on SSCBench-Waymo. All metrics and legends follow Tab. 2

5 Conclusion

Limitations and future works. SSCBench focuses on the field-of-view (FoV) in front of the vehicle, following the setup of SemanticKITTI [7] that lacks surrounding view images. Also, it only encompasses 3D data, limiting evaluations of 4D methods that incorporate temporal dimensions. Future work will aim to expand SSCBench to include panoramic viewpoints and temporal information.

Summary. In this paper, we propose SSCBench, a large-scale benchmark composed of diverse driving scenes, facilitating the development of robust and generalizable semantic scene completion models. By careful curation and comprehensive benchmarking, we identify the bottlenecks of existing methods and provide invaluable insights into future research directions. Our ambition is for SSCBench to ignite advancements in 3D semantic scene completion, fostering enhanced perception capabilities for autonomous vehicles.

References

- [1] Yiyi Liao, Jun Xie, and Andreas Geiger. Kitti-360: A novel dataset and benchmarks for urban scene understanding in 2d and 3d. *IEEE Transactions on Pattern Analysis and Machine Intelligence*, 2022. 1, 2, 3, 4
- [2] Holger Caesar, Varun Bankiti, Alex H Lang, Sourabh Vora, Venice Erin Liong, Qiang Xu, Anush Krishnan, Yu Pan, Giancarlo Baldan, and Oscar Beijbom. nuscenes: A multimodal dataset for autonomous driving. In *Proceedings of the IEEE/CVF conference on computer vision and pattern recognition*, pages 11621–11631, 2020. 1, 2, 3, 4, 7
- [3] Pei Sun, Henrik Kretzschmar, Xerxes Dotiwalla, Aurelien Chouard, Vijaysai Patnaik, Paul Tsui, James Guo, Yin Zhou, Yuning Chai, Benjamin Caine, et al. Scalability in perception for autonomous driving: Waymo open dataset. In *Proceedings of the IEEE/CVF conference on computer vision and pattern recognition*, pages 2446–2454, 2020. 1, 2, 3, 4, 8
- [4] Yiming Li, Shunli Ren, Pengxiang Wu, Siheng Chen, Chen Feng, and Wenjun Zhang. Learning distilled collaboration graph for multi-agent perception. In *Advances in Neural Information Processing Systems*, volume 34, pages 29541–29552, 2021. 1
- [5] Yiming Li, Juexiao Zhang, Dekun Ma, Yue Wang, and Chen Feng. Multi-robot scene completion: Towards task-agnostic collaborative perception. In *6th Annual Conference on Robot Learning*, 2022. 1
- [6] Luis Roldao, Raoul De Charette, and Anne Verroust-Blondet. 3d semantic scene completion: a survey. *International Journal of Computer Vision*, pages 1–28, 2022. 1, 3, 4
- [7] Jens Behley, Martin Garbade, Andres Milioto, Jan Quenzel, Sven Behnke, Cyrill Stachniss, and Jurgen Gall. Semantickitti: A dataset for semantic scene understanding of lidar sequences. In *Proceedings of the IEEE/CVF International Conference on Computer Vision*, pages 9297–9307, 2019. 1, 3, 8, 9

- [8] Scott Ettinger, Shuyang Cheng, Benjamin Caine, Chenxi Liu, Hang Zhao, Sabeek Pradhan, Yuning Chai, Ben Sapp, Charles R Qi, Yin Zhou, et al. Large scale interactive motion forecasting for autonomous driving: The waymo open motion dataset. In *Proceedings of the IEEE/CVF International Conference on Computer Vision*, pages 9710–9719, 2021. [2](#)
- [9] Yihan Hu, Jiazhi Yang, Li Chen, Keyu Li, Chonghao Sima, Xizhou Zhu, Siqi Chai, Senyao Du, Tianwei Lin, Wenhai Wang, et al. Planning-oriented autonomous driving. In *Proceedings of the IEEE/CVF Conference on Computer Vision and Pattern Recognition*, pages 17853–17862, 2023. [2](#), [3](#), [4](#), [6](#)
- [10] Andreas Geiger, Philip Lenz, and Raquel Urtasun. Are we ready for autonomous driving? the kitti vision benchmark suite. In *2012 IEEE conference on computer vision and pattern recognition*, pages 3354–3361. IEEE, 2012. [2](#), [3](#), [4](#), [7](#)
- [11] Andreas Geiger, Philip Lenz, Christoph Stiller, and Raquel Urtasun. Vision meets robotics: The kitti dataset. *International Journal of Robotics Research (IJRR)*, 2013.
- [12] Jannik Fritsch, Tobias Kuehnl, and Andreas Geiger. A new performance measure and evaluation benchmark for road detection algorithms. In *International Conference on Intelligent Transportation Systems (ITSC)*, 2013.
- [13] Moritz Menze and Andreas Geiger. Object scene flow for autonomous vehicles. In *Conference on Computer Vision and Pattern Recognition (CVPR)*, 2015.
- [14] Chao Chen, Xinhao Liu, Yiming Li, Li Ding, and Chen Feng. Deepmapping2: Self-supervised large-scale lidar map optimization. In *Proceedings of the IEEE/CVF Conference on Computer Vision and Pattern Recognition*, pages 9306–9316, 2023. [2](#)
- [15] Xinyu Huang, Xinjing Cheng, Qichuan Geng, Binbin Cao, Dingfu Zhou, Peng Wang, Yuanqing Lin, and Ruigang Yang. The apolloscape dataset for autonomous driving. In *Proceedings of the IEEE conference on computer vision and pattern recognition workshops*, pages 954–960, 2018. [2](#)
- [16] Matthew Pitropov, Danson Evan Garcia, Jason Rebello, Michael Smart, Carlos Wang, Krzysztof Czarnecki, and Steven Waslander. Canadian adverse driving conditions dataset. *The International Journal of Robotics Research*, 40(4-5):681–690, 2021. [2](#)
- [17] Siddharth Agarwal, Ankit Vora, Gaurav Pandey, Wayne Williams, Helen Kourous, and James McBride. Ford multi-av seasonal dataset. *The International Journal of Robotics Research*, 39(12):1367–1376, 2020. [2](#)
- [18] Runsheng Xu, Hao Xiang, Xin Xia, Xu Han, Jinlong Li, and Jiaqi Ma. Opv2v: An open benchmark dataset and fusion pipeline for perception with vehicle-to-vehicle communication. In *2022 International Conference on Robotics and Automation (ICRA)*, pages 2583–2589. IEEE, 2022.
- [19] Yiming Li, Dekun Ma, Ziyang An, Zixun Wang, Yiqi Zhong, Siheng Chen, and Chen Feng. V2x-sim: Multi-agent collaborative perception dataset and benchmark for autonomous driving. *IEEE Robotics and Automation Letters*, 7(4):10914–10921, 2022.
- [20] Runsheng Xu, Xin Xia, Jinlong Li, Hanzhao Li, Shuo Zhang, Zhengzhong Tu, Zonglin Meng, Hao Xiang, Xiaoyu Dong, Rui Song, et al. V2v4real: A real-world large-scale dataset for vehicle-to-vehicle cooperative perception. In *Proceedings of the IEEE/CVF Conference on Computer Vision and Pattern Recognition*, pages 13712–13722, 2023. [2](#)
- [21] Carlos A Diaz-Ruiz, Youya Xia, Yurong You, Jose Nino, Junan Chen, Josephine Monica, Xiangyu Chen, Katie Luo, Yan Wang, Marc Emond, et al. Ithaca365: Dataset and driving perception under repeated and challenging weather conditions. In *Proceedings of the IEEE/CVF Conference on Computer Vision and Pattern Recognition*, pages 21383–21392, 2022. [2](#)
- [22] Quang-Hieu Pham, Pierre Sevestre, Ramanpreet Singh Pahwa, Huijing Zhan, Chun Ho Pang, Yuda Chen, Armin Mustafa, Vijay Chandrasekhar, and Jie Lin. A 3d dataset: Towards autonomous driving in challenging environments. In *2020 IEEE International Conference on Robotics and Automation (ICRA)*, pages 2267–2273. IEEE, 2020. [2](#), [3](#)
- [23] Pengchuan Xiao, Zhenlei Shao, Steven Hao, Zishuo Zhang, Xiaolin Chai, Judy Jiao, Zesong Li, Jian Wu, Kai Sun, Kun Jiang, et al. Pandaset: Advanced sensor suite dataset for autonomous driving. In *2021 IEEE International Intelligent Transportation Systems Conference (ITSC)*, pages 3095–3101. IEEE, 2021. [2](#)
- [24] Xinyu Huang, Peng Wang, Xinjing Cheng, Dingfu Zhou, Qichuan Geng, and Ruigang Yang. The apolloscape open dataset for autonomous driving and its application. *IEEE transactions on pattern analysis and machine intelligence*, 42(10):2702–2719, 2019. [3](#)

- [25] Whye Kit Fong, Rohit Mohan, Juana Valeria Hurtado, Lubing Zhou, Holger Caesar, Oscar Beijbom, and Abhinav Valada. Panoptic nuscnescenes: A large-scale benchmark for lidar panoptic segmentation and tracking. *IEEE Robotics and Automation Letters*, 7(2):3795–3802, 2022. 3, 4
- [26] Ming-Fang Chang, John Lambert, Patsorn Sangkloy, Jagjeet Singh, Slawomir Bak, Andrew Hartnett, De Wang, Peter Carr, Simon Lucey, Deva Ramanan, et al. Argoverse: 3d tracking and forecasting with rich maps. In *Proceedings of the IEEE/CVF conference on computer vision and pattern recognition*, pages 8748–8757, 2019. 3
- [27] Jiageng Mao, Minzhe Niu, Chenhan Jiang, Jingheng Chen, Xiaodan Liang, Yamin Li, Chaoqiang Ye, Wei Zhang, Zhenguo Li, Jie Yu, et al. One million scenes for autonomous driving: Once dataset. In *Thirty-fifth Conference on Neural Information Processing Systems Datasets and Benchmarks Track*. 3
- [28] R. Kesten, M. Usman, J. Houston, T. Pandya, K. Nadhamuni, A. Ferreira, M. Yuan, B. Low, A. Jain, P. Ondruska, S. Omari, S. Shah, A. Kulkarni, A. Kazakova, C. Tao, L. Platinsky, W. Jiang, and V. Shet. Woven planet perception dataset 2020. <https://woven.toyota/en/perception-dataset>, 2019. 3
- [29] Jakob Geyer, Yohannes Kassahun, Mentar Mahmudi, Xavier Ricou, Rupesh Durgesh, Andrew S Chung, Lorenz Hauswald, Viet Hoang Pham, Maximilian Mühlegg, Sebastian Dorn, et al. A2d2: Audi autonomous driving dataset. *arXiv preprint arXiv:2004.06320*, 2020. 3
- [30] Hongyang Li, Chonghao Sima, Jifeng Dai, Wenhai Wang, Lewei Lu, Huijie Wang, Enze Xie, Zhiqi Li, Hanming Deng, Hao Tian, et al. Delving into the devils of bird’s-eye-view perception: A review, evaluation and recipe. *arXiv preprint arXiv:2209.05324*, 2022. 2
- [31] Yuexin Ma, Tai Wang, Xuyang Bai, Huitong Yang, Yuenan Hou, Yaming Wang, Yu Qiao, Ruigang Yang, Dinesh Manocha, and Xinge Zhu. Vision-centric bev perception: A survey. *arXiv preprint arXiv:2208.02797*, 2022. 2
- [32] Yue Wang, Vitor Campagnolo Guizilini, Tianyuan Zhang, Yilun Wang, Hang Zhao, and Justin Solomon. Detr3d: 3d object detection from multi-view images via 3d-to-2d queries. In *Conference on Robot Learning*, pages 180–191. PMLR, 2022. 2
- [33] Enze Xie, Zhiding Yu, Daquan Zhou, Jonah Philion, Anima Anandkumar, Sanja Fidler, Ping Luo, and Jose M Alvarez. M²2bev: Multi-camera joint 3d detection and segmentation with unified birds-eye view representation. *arXiv preprint arXiv:2204.05088*, 2022. 3
- [34] Zeyu Yang, Jiaqi Chen, Zhenwei Miao, Wei Li, Xiatian Zhu, and Li Zhang. Deepinteraction: 3d object detection via modality interaction. In *Advances in Neural Information Processing Systems*. 3
- [35] Tingting Liang, Hongwei Xie, Kaicheng Yu, Zhongyu Xia, Zhiwei Lin, Yongtao Wang, Tao Tang, Bing Wang, and Zhi Tang. Bevfusion: A simple and robust lidar-camera fusion framework. In *Advances in Neural Information Processing Systems*. 3
- [36] Tianyuan Zhang, Xuanyao Chen, Yue Wang, Yilun Wang, and Hang Zhao. Mutr3d: A multi-camera tracking framework via 3d-to-2d queries. In *Proceedings of the IEEE/CVF Conference on Computer Vision and Pattern Recognition*, pages 4537–4546, 2022. 3
- [37] Tobias Fischer, Yung-Hsu Yang, Suryansh Kumar, Min Sun, and Fisher Yu. Cc-3dt: Panoramic 3d object tracking via cross-camera fusion. In *6th Annual Conference on Robot Learning*. 3
- [38] Runsheng Xu, Zhengzhong Tu, Hao Xiang, Wei Shao, Bolei Zhou, and Jiaqi Ma. Cobevt: Cooperative bird’s eye view semantic segmentation with sparse transformers. In *6th Annual Conference on Robot Learning*, 2022. 3
- [39] Alexander Swerdlow, Runsheng Xu, and Bolei Zhou. Street-view image generation from a bird’s-eye view layout. *arXiv preprint arXiv:2301.04634*, 2023. 3
- [40] Runsheng Xu, Hao Xiang, Zhengzhong Tu, Xin Xia, Ming-Hsuan Yang, and Jiaqi Ma. V2x-vit: Vehicle-to-everything cooperative perception with vision transformer. In *European conference on computer vision*, pages 107–124. Springer, 2022. 3
- [41] Sanbao Su, Yiming Li, Sihong He, Songyang Han, Chen Feng, Caiwen Ding, and Fei Miao. Uncertainty quantification of collaborative detection for self-driving. In *IEEE International Conference on Robotics and Automation*, 2023.
- [42] Hao Xiang, Runsheng Xu, Xin Xia, Zhaoliang Zheng, Bolei Zhou, and Jiaqi Ma. V2xp-avg: Generating adversarial scenes for vehicle-to-everything perception. *arXiv preprint arXiv:2209.13679*, 2022.

- [43] Yue Hu, Yifan Lu, Runsheng Xu, Weidi Xie, Siheng Chen, and Yanfeng Wang. Collaboration helps camera overtake lidar in 3d detection. In *Proceedings of the IEEE/CVF Conference on Computer Vision and Pattern Recognition*, pages 9243–9252, 2023.
- [44] Jinlong Li, Runsheng Xu, Xinyu Liu, Jin Ma, Zicheng Chi, Jiaqi Ma, and Hongkai Yu. Learning for vehicle-to-vehicle cooperative perception under lossy communication. *IEEE Transactions on Intelligent Vehicles*, 2023.
- [45] Yiming Li, Qi Fang, Jiamu Bai, Siheng Chen, Felix Juefei-Xu, and Chen Feng. Among us: Adversarially robust collaborative perception by consensus. *arXiv preprint arXiv:2303.09495*, 2023.
- [46] Runsheng Xu, Jinlong Li, Xiaoyu Dong, Hongkai Yu, and Jiaqi Ma. Bridging the domain gap for multi-agent perception. *arXiv preprint arXiv:2210.08451*, 2022.
- [47] Sanbao Su, Songyang Han, Yiming Li, Zhili Zhang, Chen Feng, Caiwen Ding, and Fei Miao. Collaborative multi-object tracking with conformal uncertainty propagation. *arXiv preprint arXiv:2303.14346*, 2023.
- [48] Weizhe Chen, Runsheng Xu, Hao Xiang, Lantao Liu, and Jiaqi Ma. Model-agnostic multi-agent perception framework. In *2023 International Conference on Robotics and Automation (ICRA)*, 2023. 3
- [49] Lu Xiong, Xin Xia, Yishi Lu, Wei Liu, Letian Gao, Shunhui Song, and Zhuoping Yu. Imu-based automated vehicle body sideslip angle and attitude estimation aided by gnss using parallel adaptive kalman filters. *IEEE Transactions on Vehicular Technology*, 69(10):10668–10680, 2020. 3
- [50] Wei Liu, Xin Xia, Lu Xiong, Yishi Lu, Letian Gao, and Zhuoping Yu. Automated vehicle sideslip angle estimation considering signal measurement characteristic. *IEEE Sensors Journal*, 21(19):21675–21687, 2021.
- [51] Qi Li, Yue Wang, Yilun Wang, and Hang Zhao. Hdmapnet: An online hd map construction and evaluation framework. In *2022 International Conference on Robotics and Automation (ICRA)*, pages 4628–4634. IEEE, 2022.
- [52] Wei Liu, Lu Xiong, Xin Xia, Yishi Lu, Letian Gao, and Shunhui Song. Vision-aided intelligent vehicle sideslip angle estimation based on a dynamic model. *IET Intelligent Transport Systems*, 14(10):1183–1189, 2020. 3
- [53] Luis Roldao, Raoul de Charette, and Anne Verroust-Blondet. Lmscnet: Lightweight multiscale 3d semantic completion. In *2020 International Conference on 3D Vision (3DV)*, pages 111–119. IEEE, 2020. 3, 4, 5, 6, 7, 9
- [54] Ran Cheng, Christopher Agia, Yuan Ren, Xinhai Li, and Liu Bingbing. S3cnet: A sparse semantic scene completion network for lidar point clouds. In *Conference on Robot Learning*, pages 2148–2161. PMLR, 2021. 4
- [55] Christoph B Rist, David Emmerichs, Markus Enzweiler, and Dariu M Gavrila. Semantic scene completion using local deep implicit functions on lidar data. *IEEE transactions on pattern analysis and machine intelligence*, 44(10):7205–7218, 2021. 3, 4
- [56] Pengfei Li, Yongliang Shi, Tianyu Liu, Hao Zhao, Guyue Zhou, and Ya-Qin Zhang. Semi-supervised implicit scene completion from sparse lidar, 2021.
- [57] Xu Yan, Jiantao Gao, Jie Li, Ruimao Zhang, Zhen Li, Rui Huang, and Shuguang Cui. Sparse single sweep lidar point cloud segmentation via learning contextual shape priors from scene completion. In *Proceedings of the AAAI Conference on Artificial Intelligence*, volume 35, pages 3101–3109, 2021. 3
- [58] Anh-Quan Cao and Raoul de Charette. Monoscene: Monocular 3d semantic scene completion. In *Proceedings of the IEEE/CVF Conference on Computer Vision and Pattern Recognition*, pages 3991–4001, 2022. 3, 4, 5, 6, 7, 9
- [59] Yiming Li, Zhiding Yu, Christopher Choy, Chaowei Xiao, Jose M Alvarez, Sanja Fidler, Chen Feng, and Anima Anandkumar. Voxformer: Sparse voxel transformer for camera-based 3d semantic scene completion. In *Proceedings of the IEEE/CVF Conference on Computer Vision and Pattern Recognition*, pages 9087–9098, 2023. 4, 5, 6, 7, 8, 9
- [60] Yuanhui Huang, Wenzhao Zheng, Yunpeng Zhang, Jie Zhou, and Jiwen Lu. Tri-perspective view for vision-based 3d semantic occupancy prediction. In *Proceedings of the IEEE/CVF Conference on Computer Vision and Pattern Recognition*, pages 9223–9232, 2023. 3, 4

- [61] Shuran Song, Fisher Yu, Andy Zeng, Angel X Chang, Manolis Savva, and Thomas Funkhouser. Semantic scene completion from a single depth image. In *Proceedings of the IEEE conference on computer vision and pattern recognition*, pages 1746–1754, 2017. 3, 5, 6, 7, 9
- [62] Sebastian Thrun. Probabilistic robotics. *Communications of the ACM*, 45(3):52–57, 2002. 3
- [63] Sean L Bowman, Nikolay Atanasov, Kostas Daniilidis, and George J Pappas. Probabilistic data association for semantic slam. In *2017 IEEE international conference on robotics and automation (ICRA)*, pages 1722–1729. IEEE, 2017. 4
- [64] Xiaoshuai Zhang, Abhijit Kundu, Thomas Funkhouser, Leonidas Guibas, Hao Su, and Kyle Genova. Nerflets: Local radiance fields for efficient structure-aware 3d scene representation from 2d supervision. In *Proceedings of the IEEE/CVF Conference on Computer Vision and Pattern Recognition*, pages 8274–8284, 2023. 4
- [65] Junru Gu, Chenxu Hu, Tianyuan Zhang, Xuanyao Chen, Yilun Wang, Yue Wang, and Hang Zhao. Vip3d: End-to-end visual trajectory prediction via 3d agent queries. In *Proceedings of the IEEE/CVF Conference on Computer Vision and Pattern Recognition*, pages 5496–5506, 2023. 4
- [66] Yiming Li, Congcong Wen, Felix Juefei-Xu, and Chen Feng. Fooling lidar perception via adversarial trajectory perturbation. In *Proceedings of the IEEE/CVF International Conference on Computer Vision*, pages 7898–7907, 2021. 4
- [67] Tim Bailey and Hugh Durrant-Whyte. Simultaneous localization and mapping (slam): Part ii. *IEEE robotics & automation magazine*, 13(3):108–117, 2006. 5
- [68] Daniel Maturana and Sebastian Scherer. Voxnet: A 3d convolutional neural network for real-time object recognition. In *2015 IEEE/RSJ international conference on intelligent robots and systems (IROS)*, pages 922–928. IEEE, 2015. 5
- [69] Yin Zhou and Oncel Tuzel. Voxelnet: End-to-end learning for point cloud based 3d object detection. In *Proceedings of the IEEE conference on computer vision and pattern recognition*, pages 4490–4499, 2018. 5
- [70] Shariq Farooq Bhat, Ibraheem Alhashim, and Peter Wonka. Adabins: Depth estimation using adaptive bins. In *Proceedings of the IEEE/CVF Conference on Computer Vision and Pattern Recognition*, pages 4009–4018, 2021. 7
- [71] Faranak Shamsafar, Samuel Woerz, Rafia Rahim, and Andreas Zell. Mobilestereonet: Towards lightweight deep networks for stereo matching. In *Proceedings of the IEEE/CVF Winter Conference on Applications of Computer Vision*, pages 2417–2426, 2022. 7
- [72] Ning Zhang, Francesco Nex, George Vosselman, and Norman Kerle. Lite-mono: A lightweight cnn and transformer architecture for self-supervised monocular depth estimation. In *Proceedings of the IEEE/CVF Conference on Computer Vision and Pattern Recognition*, pages 18537–18546, 2023. 7, 8